Tectonophysics 836 (2022) 229405

Contents lists available at ScienceDirect

Tectonophysics

journal homepage: www.elsevier.com/locate/tecto

Estimation of the maximum earthquakes magnitude based on potential brittle volume and strain rate: The Italy test case

P. Petricca [a,*,1], E. Carminati [a], C. Doglioni [a,b]

[a] Dipartimento di Scienze della Terra, Università Sapienza, Roma, Italy
[b] Istituto Nazionale di Geofisica e Vulcanologia, Roma, Italy

ARTICLE INFO

Keywords:
Seismic hazard assessment
Earthquakes
Seismic volume
Graviquakes
Elastoquakes
Italian seismicity

ABSTRACT

One major critical issue in seismic hazard analysis deals with the computation of the maximum earthquake magnitude expected for a given region. Its estimation is usually based on the analysis of past seismicity that is incomplete by definition, or derived from the dimension of faults through empirical relationships with the intrinsic uncertainty in source characterization. Here, we propose a workflow aimed at providing a time-independent estimate for the maximum possible magnitude based on geological and geophysical evidence. Our estimate is also source unrelated as it is constrained by the seismic brittle volume of the crust that scales with the effective seismic energy. The seismic brittle volume is calculated considering fault kinematics and rock rheology (i.e., the brittle-ductile transition depth) over a grid that covers the entire study area. The maximum earthquake magnitude is calculated at each point of the grid based on a volume/magnitude empirical relationship. We apply this model to Italy for which we propose a map of the maximum possible magnitudes. Maximum predicted magnitudes are 7.3 ± 0.25 for thrust faulting, 7.6 ± 0.77 for normal faulting and 7.6 ± 0.37 for strike-slip faulting (± deviation from the mean value calculated at each node). These magnitudes are locally higher than the historical record. This could be due to an overestimation of the involved volumes; smaller volumes and lower magnitudes may occur where faults are detached at decollements shallower than the brittle ductile transition or where they behave aseismically. Alternatively, strong or major earthquakes could be possible, but they have longer recurrence time and they have never been recorded yet in Italy. Regardless these values are fully reliable or not, the recurrence of earthquakes with the predicted magnitude is related to current strain rates. We conclude that a large part of the Italian territory is prone to trigger Mw > 5 earthquakes.

1. Introduction

The elastic rebound theory (Reid, 1910), mathematically described by Ohnaka (1976), assumes that faults obey regular patterns of behavior. This idea, which is based on the assumptions of characteristic earthquakes (e.g., Aki, 1984; Schwartz and Coppersmith, 1984) inherently backgrounds the work of earthquake research and forecasting since the 20th century. In some cases, the assumption underlying this hypothesis, at the base of predictions of maximum magnitudes of individual large events used to produce probabilistic hazard maps, is that faults are "predictable" in the sense that they tend to rupture with the same size and mechanism (e.g. Kammerer and Ake, 2012) and that big earthquakes are most likely to strike in seismic gaps. These concepts are implicitly time-dependent and practically led to estimations of maximum magnitudes mainly based on past seismicity (Atkinson, 2004) from catalogs that are incomplete by definition (e.g., Mohammed et al., 2014; Wyss, 2015). This approach is very diffuse worldwide for the preparation of official hazard maps (e.g., the SESAME for Mediterranean basin - Jimenez et al., 2001; The United States national seismic hazard model – Petersen et al., 2015; the New Zealand national Seismic Hazard Model – Stirling et al., 2012). Hybrid approaches to estimate the maximum magnitude were proposed in order to bypass the limited time-span of seismic catalogs selecting the larger magnitude between that reported in the seismic record and that derived from fault dimension through empirical relationships (e.g., the European Seismic Hazard Model ESHM13 – Woessner et al., 2015; the Italian Seismic Hazard Model MPS19 - Meletti et al., 2021; Visini et al., 2021). In the Database of Individual Seismogenic Sources of Italy (DISS Working Group, 2021)

* Corresponding author.
E-mail address: patrizio.petricca@uniroma1.it (P. Petricca).
[1] Current address: ISPRA - Servizio Geologico d'Italia, Roma, Italy.

https://doi.org/10.1016/j.tecto.2022.229405
Received 31 January 2022; Received in revised form 4 May 2022; Accepted 10 May 2022
Available online 18 May 2022

and the European Database of Seismogenic Sources (Basili et al., 2013) maximum magnitude values proposed in the literature from detailed studies are also integrated. However, due to earthquakes' long recurrence times, these approaches may fail to consider largest magnitude events for a given location because not yet observed, hence producing underestimation of the resulting hazard (Scholz, 2019). This typically applies to regions uninhabited during historical times and now densely populated or where the recurrence time of strong earthquakes is much longer than the onset of the seismological record (Trippetta et al., 2019 and references therein). In fact, seismologists often face with the occurrence of unexpected (or uncharacteristic; Geller et al., 2015 and references therein) earthquakes that highlight the incompleteness of these approaches, which often fail (see Wyss, 2015) to predict both earthquakes magnitude, peak ground acceleration and recurrence interval (e.g., Tohoku 2011 Mw 9 instead of the predicted Mw 7.5 characteristic earthquake; Italy 2012 Mw 6.1 produced up to 0.3 g of ground acceleration instead of 0.125–0.150 g - 10% in 50 yrs - predicted by the official seismic hazard model; Parkfield earthquake expected at 95% probability before 1993 occurred in 2004 with ambiguities in location and characteristics with respect of what it was predicted). Moreover the concept of Maximum Credible Earthquake (MCE) has also been introduced, which is based on seismic history and seismotectonics and is a basic ingredient for a neodeterministic technique (NDSHA) to calculate the seismic hazard (e.g., Panza and Bela, 2020).

To avoid the problem of time-dependence, the maximum magnitude of earthquakes can be assessed using empirical scaling relationships that relate active faults characteristics (generally fault length and/or fault slip) to the maximum magnitude expected in case of the rupture of the whole length of that fault (Wells and Coppersmith, 1994; Mai and Beroza, 2000; Leonard, 2010, 2014; Thingbaijam et al., 2017; Schirripa Spagnolo et al., 2021). In this latter case a big problem is the uncertainty in source characterization (e.g., Schwartz, 2018). Criteria for selection of active faults are even more markedly subjective. Further, where strain rates are low to intermediate and faults are small in dimensions and unclear in surface expression of recent activity, the connection between faults and earthquakes is not straightforward (Trippetta et al., 2019).

Here, we propose a model for an alternative methodology to calculate the maximum magnitude expected for a region. The method is based on an invariant (on human time-scales) characteristic of the system, that is the available brittle volume, thus providing the maximum possible magnitude (i.e. the upper energy limit). This way may overcome the incompleteness of the seismic catalogs and the uncertainty in source characterization, since the effective potential is unrelated to the dimension of the faults (see Doglioni et al., 2015; Petricca et al., 2015, 2018, 2019). The maximum magnitude is calculated at each node of a 10 km × 10 km regular grid covering the study area and is strictly time-independent with recurrence related to strain rates. The present study integrates and extends findings of previous papers where the model was preliminary applied to extensional areas (Petricca et al., 2015) and compressional areas (Petricca et al., 2019) of Italy. In this new version we propose a map of maximum possible magnitudes that covers all the kinematic regions of Italy (i.e. with extension, compression and strike-slip tectonics). Since our map provides a first estimate of the maximum magnitude, we preferred to investigate only well-constrained tectonic regions. Therefore we excluded Sardinia and Apulia, aware that these areas are potentially seismic due to the presence of faults with recent tectonic activity (see, for Sardinia, Casula et al., 2001; for Apulia Argnani et al., 2001) and moderate earthquakes in historical record with Mw ~5 (e.g. south Sardegna 1616; Rovida et al., 2021) or even Mw >6 (e.g., Salento-Apulia 1743; Galli and Naso, 2008; Nappi et al., 2017). Small geodetic rates for these regions (<1 mm/yr; Devoti et al., 2017; Farolfi and Del Ventisette, 2017) imply that the recurrence interval of large events would be very large. Our map is a step forward with respect to previous works because it relies: 1) on a brittle-ductile transition depth (BDT) map updated with respect to that proposed in Petricca et al. (2015), that is the basis for brittle volumes estimation in extensional and strike-slip areas; 2) an updated version - with respect to that proposed in Petricca et al. (2019) - of the map of the thrusts decollement depth necessary for calculation of brittle volumes in compressional areas; 3) a more recent solution for GPS record (Devoti et al., 2017) used to compute the BDT depth and to define the annual rates of strain.

The map of the maximum possible magnitude of Italy is then i) compared with maximum magnitudes used to produce the Italian Seismic Hazard Model MPS19 (Meletti et al., 2021; Visini et al., 2021), and then ii) tested versus the geodetic strain rate with the scope of delimiting areas of maximum probability for next moderate/large earthquakes occurrence.

2. Seismotectonics of Italy

Italy is located along a complex plate boundary where at least three main plates (Eurasia, Africa and Adria) interact (Carminati and Doglioni, 2012). Recorded earthquakes allow the recognition of extensional, compressional and transcurrent stress fields (Fig. 1). The coexistence of these different tectonic regimes is the result of active subduction processes building up two mountain chains (Alps and the Apennines) and producing the Apennines back-arc extension (Carminati and Doglioni, 2012; Malinverno and Ryan, 1986). The Alps (characterized by double vergence and high elevation) and the Apennines (verging mostly eastward) belts grew on top of subduction zones characterized by slab hinges converging and diverging relative to the upper plates, respectively. The rates of motion at the surface from GPS data are in the order of a few mm/yr (Devoti et al., 2017). Contractional deformation concentrates along the front of the Southern Apennines, the eastward offshore of Calabria, the south Tyrrhenian Basin and, mainly, along the central-northern Adriatic margins and between the Northern Apennines and the Southern Alps (Fig. 1). To the west of the active Apennines accretionary prism, the Apennines are characterized by extensional tectonics. Here, previous contractional structures (thrust faults and folds) are crosscut by active normal faults (Carminati and Doglioni, 2012). In the frontal accretionary prism and in the backarc basin, strike-slip faults mostly play a subsidiary role of transfer zones, whereas in the foreland, lithospheric transcurrent faults act as tear zones accommodating differential slab retreat in areas where strong earthquakes may occur (e.g., the Gargano and the Malta escarpment areas).

Historical and instrumental catalogs show a dense distribution of seismicity in Italy (Fig. 1), that has been struck by numerous moderate to strong earthquakes (Rovida et al., 2021). The most energetic earthquakes (Fig. 1) are concentrated along the extensional ridge of the Apennines where Mw exceeding 6 are frequent (e.g., Colfiorito 1997, Mw 6.0 - Amato et al., 1998; Norcia 2016 Mw 6.5 and Amatrice 2016 Mw 6.0 - Chiaraluce et al., 2017; L'Aquila 2009, Mw 6.3 -Chiarabba et al., 2009; Irpinia 1980, Mw 6.8 - Rovida et al., 2021). Large thrust earthquakes, though less numerous, were recorded in the eastern Alps (Friuli earthquake with Mw = 6.4 in 1976 - Caputo, 1976) and, possibly, in the Po Plain (1117, with Mw 6.5, although fault kinematics is not constrained - Guidoboni et al., 2005; 2012 with Mw 6.1 - Govoni et al., 2014). Although its focal mechanism remains unknown, the largest historical earthquake ever recorded in Italy has struck southeastern Sicily in 1693 (M 7.3 - https://emidius.mi.ingv.it/CPTI15-DBMI15).

3. Data and methods

The proposed procedure for the evaluation of the maximum possible magnitude, here applied to the Italian region, foresees that, via available geological and geophysical data, we define: 1) the extent of areas characterized by compressional, extensional and strike-slip tectonics; 2) the relationship between length of possible ruptures (L_f) for seismogenic faults and the maximum faulting depth (z_{max}) of related earthquakes - that varies from $L_f/z_{max} = 2$ to $L_f/z_{max} = 25$ depending on the tectonic regime and on the strain rate (Doglioni et al., 2015; Petricca et al., 2018; Petricca et al., 2019); 3) the maps of the active thrust decollement depth

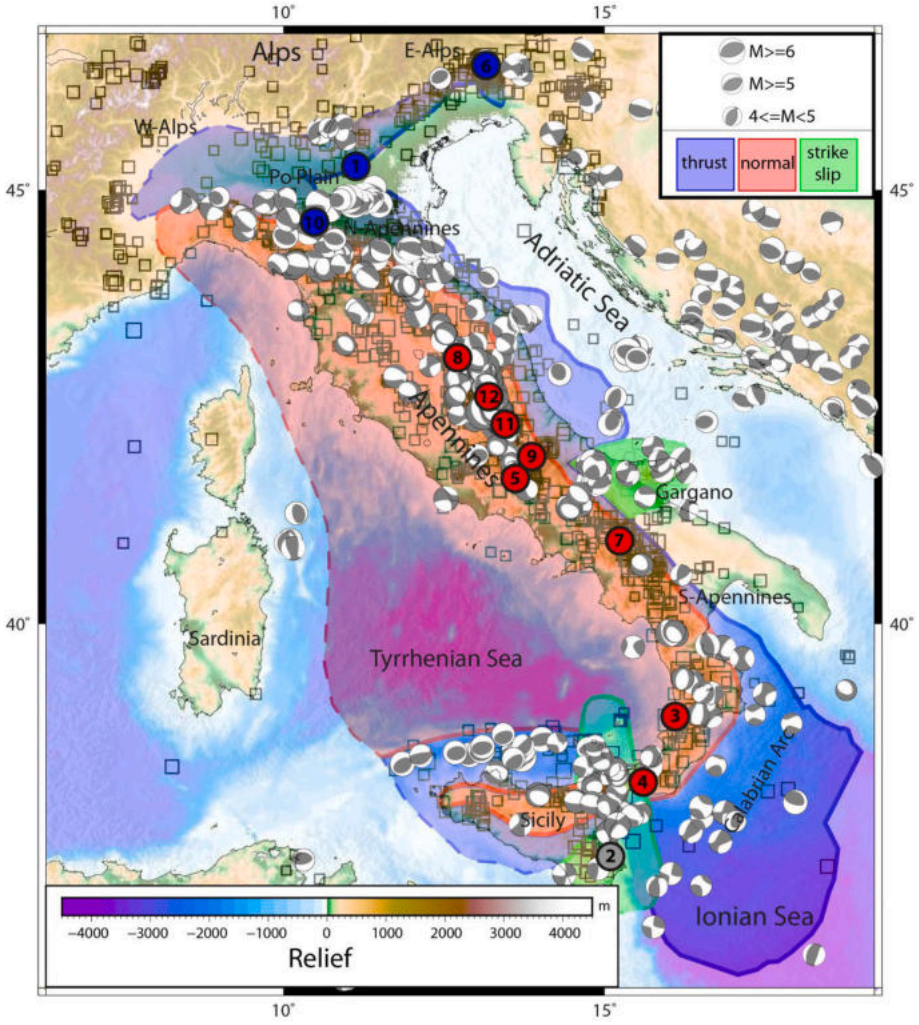

Fig. 1. Focal mechanisms of major instrumentally recorded earthquakes in Italy with Mw ≥ 4 (1997–2021 from the rCMT catalog; Pondrelli et al., 2006) and (gray squares) earthquakes from the CPTI15 catalog with Mw ≥ 4 (from year 1005 to 2019); the most energetic earthquakes are evidenced by blue (compressional), red (extensional), gray (unknown) solid circles: 1- Veronese 1117 M_w 6.5; 2- SE-Sicily 1693 M_w 7.3; 3- Calabria 1905 M_w 7; 4- Calabria 1908 M_w 7.1; 5- Fucino 1915 M_w 7.1; 6- Friuli 1976 M_w 6.4; 7- Irpinia 1980 Mw 6.9; 8- Colfiorito 1997 M_w 6.0; 9- L'Aquila 2009 M_w 6.3; 10- Emilia 2012 M_w 6.1; 11- Amatrice 2016 M_w 6.0; 12- Norcia 2016 M_w 6.5. Blue areas represent regions of compression associated with the front of the Southern Alps fold-and thrust belt and the front Apennines-Maghrebian accretionary prism; red areas are regions of Apennines extension and Tyrrhenian back-arc spreading; green areas are those dominated by strike-slip tectonics. (For interpretation of the references to colour in this figure legend, the reader is referred to the web version of this article.)

(for compressional area; Petricca et al., 2019 and this study; Table S1) and brittle-ductile transition depth (BDT for extensional and strike-slip areas; Petricca et al., 2015 and this study; Table S2). In fact, normal fault ruptures can propagate through the entire seismogenic crust, whereas thrusts frequently flatten along regional detachments and do not cut down to the brittle-ductile transition, requiring different definitions of maximum faulting depth for the two regimes. With parameters from points 1) to 3) we calculate 4) the seismogenic brittle volume and, by means of empirical relationship 5) the maximum potential magnitude based on the potential seismogenic volume. Eventually, 6) regions with maximum probability of future moderate/large earthquakes occurrence are delimited, depending on the present strain rate. The map of the maximum possible magnitude in Italy based on the seismogenic brittle volume is finally proposed.

3.1. Areal extent of compression, tension and strike-slip deformation

Boundaries of compressional regions (blue boxes in Fig. 1) are modified from Petricca et al. (2019) while extensional and strike-slip areas (red and green boxes in Fig. 1) are modified from Petricca et al. (2015). Homogeneous kinematic areas are defined by integrating the location of Apennines and Alps thrust fronts from literature (Carminati and Doglioni, 2012; Petricca et al., 2013), GPS data and the geometry of composite seismogenic sources from the database of the individual seismogenic sources of Italy (DISS - DISS Working Group, 2021). The closure of polygons is obtained by considering horizontal GPS velocity field along the transects published in Petricca et al. (2015), i.e., selecting the points separating extensional/contractional fields along the whole study domain.

3.2. The length - maximum fault depth ratio (C) and dip angles of Italian faults

The first assumption of our method is that fault ruptures show a well-defined shape ratio (C) between fault length (L_f) and maximum fault depth (z_{max}), that is dependent on fault-type (extensional, compressional or strike-slip). C values are here derived from individual seismogenic sources (ISS) given in the DISS database (DISS Working Group, 2021). From DISS we selected all the 43 ISSs with thrust/transpressional kinematics (i.e., 45° < rake angle <135°), the 59 ISSs with normal/transtensional kinematics (i.e., 225° < rake angle <315°) and all the 21 ISSs with strike slip kinematics (i.e., 135° ≤ rake angle ≤225°, rake angle ≥315° and rake angle ≤45°). The given values for the minimum and maximum source depth (Min depth and Max depth in the DISS nomenclature) and the source rupture length (L_f) are used to calculate the ratio between fault length and the maximum depth of faulting $L_f/z_{max} = L_f/(\text{Max depth - Min depth})$. Values for normal faults are distributed around L_f/z_{max} = 1–3 (Fig. 2a), for thrust faults around L_f/z_{max} = 1–4 (Fig. 2b) while for strike-slip are L_f/z_{max} = 1–2 (Fig. 2c). L_f/z_{max} ratio increases with the magnitude and the rupture length. We use obtained L_f/z_{max} ranges (L_f/z_{max} = 1–3 and L_f/z_{max} = 1–4 for normal and thrust faults respectively) as end-members in the following

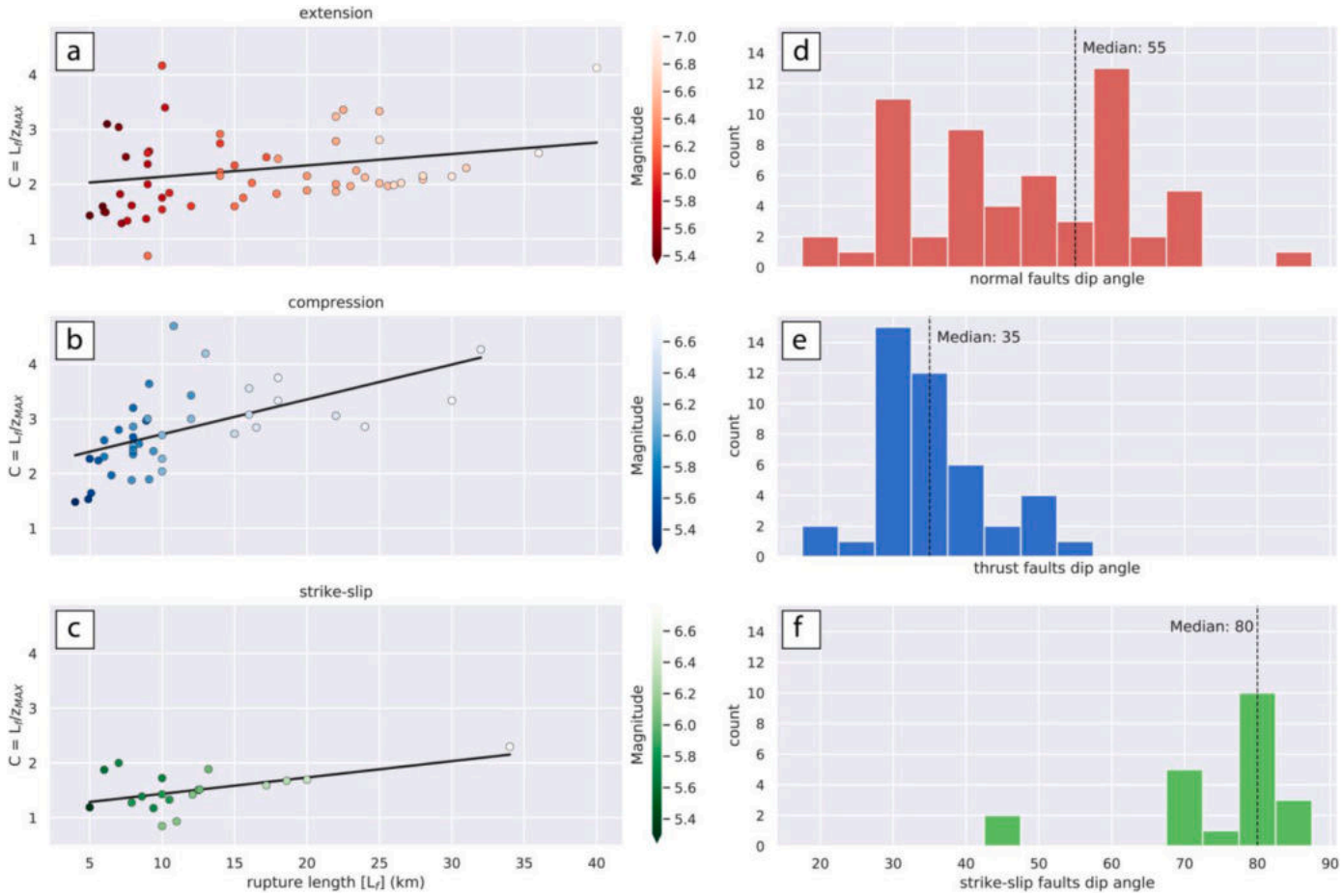

Fig. 2. Rupture length (L_f) against the $C = L_f/z_{max}$ ratio for known **a)** normal, **b)** thrust and **c)** strike-slip sources in Italy (listed in Table S4) colored according to the magnitude. $C = L_f/z_{max}$ increases with the magnitude and the rupture length, as shown by regression lines (black solid lines). Values extrapolated from the DISS database regarding the fault dip values observed for the three different regimes. Histograms highlight that the minimum and maximum fault dips are: **d)** 20°-85° (normal faults), **e)** 20°-55° (thrust faults) and **f)** 45°-88° (strike-slip faults). The median values are 55°, 35° and 80° respectively. Notice that the maximum and minimum values are used as upper and lower bounds in brittle volume calculation (see main text) while we consider the medians as reference for the preferred model of the map of maximum possible magnitudes (see Fig. 7).

computations of the maximum seismogenic volume. The value obtained for strike slip faults ($L_f/z_{max} = 1–2$) is constrained by very few events and is at odds with detailed studies for strike-slip events in Italy (e.g., Fracassi and Valensise, 2007; Valensise et al., 2004). For the sake of completeness, based on the literature we extended the range for strike-slips faults up to $L_f/z_{max} = 3$.

From the same DISS database we extrapolated the maximum and minimum fault dip values for the three different regimes that are: 20°-85° (normal), 20°-55° (thrust) and 45°-88° (strike-slip); the median values are 55°, 35° and 80° respectively (Fig. 2d-f). The maximum and minimum values are used as upper and lower bounds in brittle volume calculation while we consider the medians as the reference value in the resulting preferred map of maximum possible magnitudes. However, our calculations are extended to different fault dip values.

3.3. Decollement depth and Brittle-Ductile Transition Depth (BDT)

The maximum volume that can be activated during the seismic cycle is constrained by the depth of the brittle-ductile transition (BDT) or by the depth of the decollement of the basal active thrust (Petricca et al., 2015, 2019). Normal fault rupture tends to propagate upward cutting the brittle crust (Carminati et al., 2004). However, normal faults may flatten shallower than the brittle-ductile transition depth into low-angle faults cutting throughout low friction formations as it occurred in the 2016–2017 Mw6.5 Amatrice-Norcia central Italy seismic sequence (Carminati et al., 2020). Also thrust faults may not necessarily cut down to the brittle-ductile transition (Hyndman et al., 1997). It follows that, for different seismotectonic areas of Italy (Fig. 1), we utilize two different approaches that consider i) the map of the brittle-ductile transition (BDT) depth for extensional and strike-slip tectonics, and ii) the map of the active thrusts decollement depth for compressional tectonics (Fig. 3). The map of BDT depth is used to calculate brittle volumes in the extensional/strike-slip domains and is produced following the procedure described in Petricca et al. (2015); is based on the same base parameters that are the heat flow (from Della Vedova et al., 2001), the crustal thickness (from Mele et al., 2013; Carafa and Barba, 2011), and the strain rate. The version of the map presented in this study is recomputed considering the last available solution for the strain rate (SR) obtained using updated GPS data (Devoti et al., 2017) with respect to the old solution used in Petricca et al. (2015). The thickness of the brittle layer of the upper crust is calculated on a 10 × 10 km grid based on the thermal profile calculated at each node. The map of the decollement depth is recomputed from Petricca et al. (2019), integrating data from compressional areas of Italy not considered in the previous version. The traces of the geological cross-sections utilized in this study are displayed in red in Fig. 3 and include datasets from Cassano et al. (1986), Merlini et al. (2002), Pezzo et al. (2020), Schönborn (1999), Scrocca (2006) and Doglioni and Carminati (2008).

Due to the fact that the brittle-ductile transition (BDT) depth is possibly and locally shallower than the basal thrust depth (Petricca

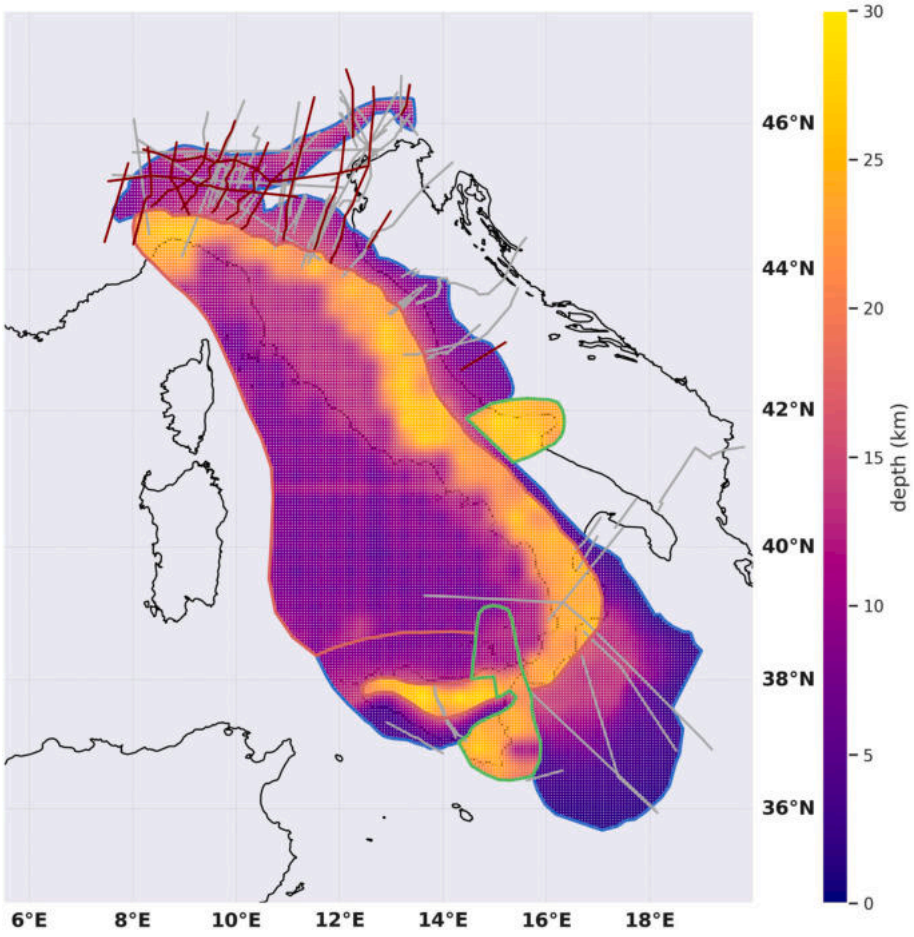

Fig. 3. Map of the brittle-ductile transition depth (after Petricca et al., 2015) plotted for extensional (bordered in light red) and strike-slip (bordered in green) areas merged with the map of the maximum thrust faulting depth calculated for compressional areas of Italy (after Petricca et al., 2019). Traces of geologic sections used for decollement depth definition in Petricca et al. (2019) are reported in dark gray; traces of new geologic sections from Cassano et al. (1986), Merlini et al. (2002), Pezzo et al. (2020), Schönborn (1999) and Scrocca (2006) integrated in this study are reported in red. (For interpretation of the references to colour in this figure legend, the reader is referred to the web version of this article.)

et al., 2019), we compare the BDT depths with the basal thrust depths selecting at each node of the compressional areas the shallower value. The BDT is shallower than the basal thrust depth in the southern Tyrrhenian Sea (off-shore Sicily).

3.4. The seismogenic brittle volume

The maximum volume that can be mobilized by a fault during the coseismic stage is quantifiable a priori. It is possible to approximate it to a triangular-base prism since it describes the deformed epicentral area determined by the volume size and the related fault length, depth and dip (Petricca et al., 2021). The volume of the prism can be obtained by considering the length of a hypothetic master fault, that is proportional to C (length - fault depth ratio; see section 3.2), multiplied by the maximum faulting depth z_{max} (BDT or decollement depth) and by a conjugated fault dipping 90° opposite to the master fault (see Petricca et al., 2015 and Petricca et al., 2019 for better explanation). Brittle volumes are calculated over a regular grid of 10 km × 10 km for the whole Italian territory. This approach aims at constraining the upper limit of the seismic energy potentially available for a given region (i.e. the maximum possible brittle volume) irrespective of the detail of knowledge of the area (e.g., the presence of blind seismogenic faults or fault inactivity longer than historic record are overcome). The height of the prism is assumed to be equal to the BDT depth for normal and strike-slip faults and to the active decollement depth for thrust faults. The volume is calculated using the relationship (Petricca et al., 2019):

$$1) \quad V = \frac{C}{2} z^3_{max} [cot(\alpha) + cot(90 - \alpha)]$$

where α is the fault dip (20° to 55° for thrust, 20° to 85° for normal and 45° to 88° for strike-slip faults), z_{max} is the deepest tip of the activation of a seismogenic thrust or the BDT depth along a seismogenic normal or strike-slip fault, C is the L_f/z_{max} ratio (1 to 4 for thrust, 1 to 3 for normal and strike-slip faults). Brittle volumes up to about $1.7 \bullet 10^4$ km^3 are obtained in compressional areas assuming a fault dip of 35° (i.e. the median value characterizing active thrusts in Italy) and considering C = 4. Brittle volumes up to $7.8 \bullet 10^4$ km^3 are obtained in extensional areas assuming a fault dip of 55° (i.e., the median value) and considering C = 3. Brittle volumes up to $6.4 \bullet 10^4$ km^3 are obtained in strike-slip areas assuming a fault dip of 80° (i.e., the median value) and considering C = 1 (Fig. 4). The full range of variation of maximum brittle volumes obtained by changing initial parameters (fault dip angles α and shape ratio C) are summarized in Table 1 and collected in Table S3.

3.5. Maximum potential magnitude and tectonic regime

In extensional settings, gravity favors faulting because, according to Anderson's model (Anderson, 1951), the maximum stress axis is approximately parallel to the lithostatic load. The lithostatic load rather buffers (i.e., counteracts) the elastic energy accumulated during the interseismic period in thrust or strike-slip faulting. The elastic rebound is commonly considered as the main model for earthquake generation, being inferred as the mechanism dissipating the elastic energy accumulated during the interseismic period. This is likely true for contractional and strike-slip tectonic settings, but in extensional environments, the influence of gravity may rather be dominant (Doglioni et al., 2011; Bignami et al., 2020). The occurrence of different mechanisms controlling earthquakes in different tectonic settings must be considered when calculating magnitudes expected from a potential brittle volume. A linear correlation was proposed between earthquake magnitudes and

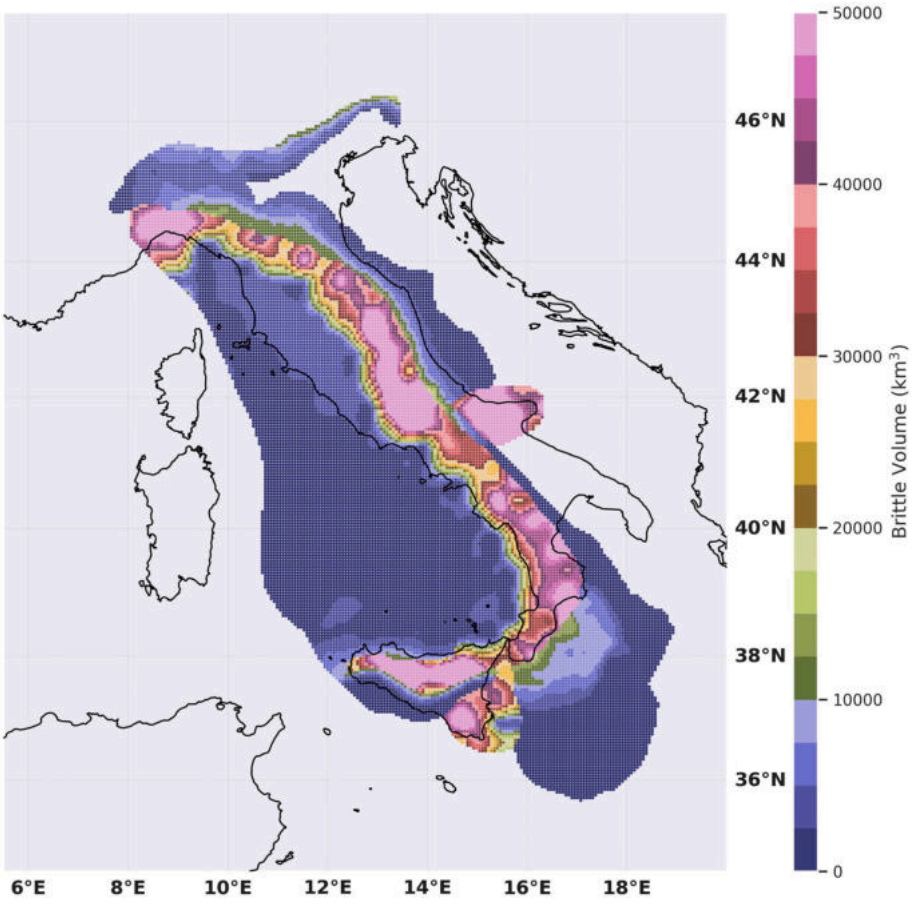

Fig. 4. Map of the brittle volumes of the Italian territory involved in compressional, extensional and strike-slip areas. Brittle volume is calculated assuming the following fault dip α and $C = L_f/z_{max}$ (i.e. fault length - maximum faulting depth ratio): α =35° and C = 4 (thrust faults); α =55° and C = 3 (normal faults); α =80° and C = 1 (strike-slip faults). This map represents the brittle volume that can be mobilized during earthquakes by hypothetical faults.

Table 1
Calculated brittle volumes and Maximum possible Magnitudes for normal (N), thrust (T) and strike-slip (SS) faults depending on initial parameters assumption (fault dip angle and Lf/zmax ratio C).

	Brittle volume ($km^3 \bullet 10^4$) (dip angle; L_f/z_{max})		Maximum possible magnitude	
	$Range_{min}$	$Range_{max}$	$Range_{min}$	$Range_{max}$
N	0.01–3.8 (α = 20°; C = 1)	0.01–42.3 (α = 85°; C = 3)	4.3–7.1 (α = 20°; C = 1)	4.1–8.7 (α = 85°; C = 3)
T	0.0001–0.4 (α = 55°; C = 1)	0.0001–2.6 (α = 20°; C = 4)	3.8–7.4 (α = 55°; C = 1)	3.9–8.0 (α = 20°; C = 4)
SS	0.01–2.2 (α = 45°; C = 1)	0.2–25.3 (α = 85°; C = 1)	5.6–7.6 (α = 45°; C = 1)	6.0–8.0 (α = 85°; C = 1)

the logarithm of the seismogenic volume (Bath and Duda, 1964; Petricca et al., 2015, 2019). The maximum potential magnitude (M) can be calculated as (Bath and Duda, 1964):

$$2) \quad M_{BD} = log\,(V) - 9.58/1.47$$

where V is the brittle volume in cm^3. M_{BD} is appropriate for thrust and strike-slip areas, but it does not consider the role of the gravitational potential, that is dominant in extensional tectonic, for which we can introduce the potential residual energy RU:

$$3) \quad RU = \rho V g(1 - \mu \cos\alpha)u_s$$

where ρV is the mass of a volume V (km^3) having density ρ (we adopt average value for continental crust 2600 kg/m^3; Dziewonski and Anderson, 1981); μ is the fault friction coefficient (0.6 according to Byerlee, 1978), u_s the average coseismic slip (in m) and α the assumed fault dip. For extensional areas, the maximum possible magnitude is calculated as (Choy and Boatwright, 1995):

$$4) \quad M_{CH} = \frac{2}{3} log(RU \times r_c) - 3.2$$

where r_c is the seismic radiation coefficient (Aki and Richards, 1980) here assumed equal to 1.0 (Choy and Boatwright, 1995; Doglioni et al., 2011). Since the gravity force must be considered in extensional tectonics we calculate M_{CH} for extensional areas. M_{BD} is more appropriate to be computed in thrust and strike-slip areas.

Petricca et al. (2018) showed that for thrust tectonics (i.e., where elastic force dominates) a given brittle volume has a potential magnitude that increases by 1 when the shortening rate is 10 times faster. Italy (excluding volcanic areas) is characterized by strain rates in the range of 1 to 5 mm/yr (Devoti et al., 2017). We used velocities interpolated from Devoti et al. (2017) (Fig. 5) to correct the maximum magnitudes predicted in compressional and strike-slip areas. The velocity has been normalized in the 0–1 range and added to the magnitude obtained by volumetric constraints. Eventually, we get that the maximum magnitude predicted by our model depends on the brittle volume plus the gravitational potential in extensional areas and on the brittle volume plus the strain rate in compressional and strike-slip areas. The difference in methodology is consistent with the fact that, in the brittle volume - predicted magnitude diagram of Fig. 6, the magnitudes calculated at each node with our preferred model are aligned along a curve for

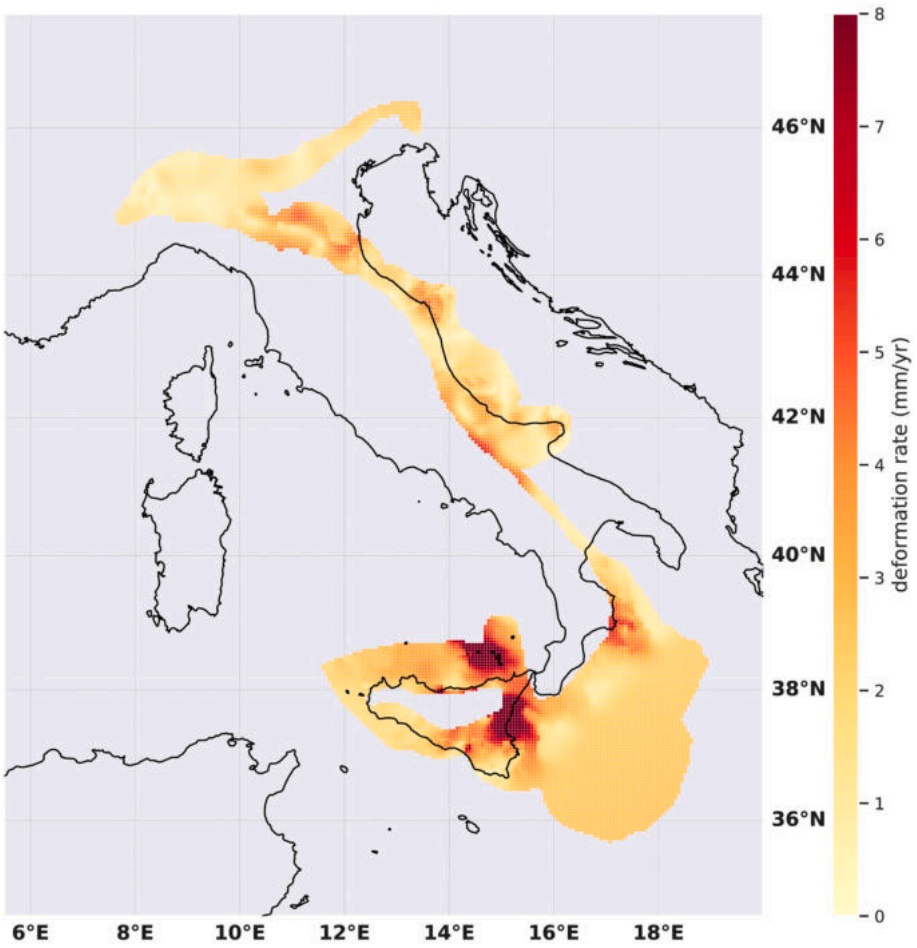

Fig. 5. Strain rate from GPS velocity (after Devoti et al., 2017) used to calculate maximum magnitudes of Fig. 7 for compressional and strike-slip areas of Italy.

extensional tectonic settings (red curve), while for compressional and strike-slip tectonic settings, for which the same brittle volume can predict different magnitudes depending on the strain rate, the calculated magnitudes occur in bands (blue for compression; green for strike-slip).

4. The maximum potential magnitude of Italy

The map of magnitudes calculated from maximum brittle volumes is presented in Fig. 7 for well constrained areas of Italy (compressional, extensional and strike-slip areas; Table S3) assuming the following values for geometric parameters: a fault dip of 35° (thrust), 55° (normal) and 80° (strike-slip), $L_f/z_{max} = 4$ (thrust), $L_f/z_{max} = 3$ (normal) and $L_f/z_{max} = 1$ (strike-slip). According to the model presented here, the maximum potential magnitude in regions under tension ranges between 4.5 and 7.6. Magnitudes between 4.3 and 7.1 are obtained considering $L_f/z_{max} = 1$ while magnitude range increases to 4.1–8.7 considering $L_f/z_{max} = 3$ and increasing the fault dip to 85° (Fig. 8a and Table 1). The maximum magnitude is predicted along the Apennines axis, i.e. where the brittle layer is thicker (Fig. 3) and the most recent energetic normal earthquakes of Italy are concentrated (e.g. Colfiorito 1998 Mw = 6.0; Norcia Mw = 6.5 and Amatrice Mw = 6.02016; L'Aquila 2009 Mw = 6.3; Irpinia 1980 Mw = 6.9). Even larger earthquakes characterize the Southern Apennines area, with historical events that reached magnitudes up to 7.3 (see section 2 for references).

In thrust-fault settings, a 3.8–7.8 potential magnitude range is obtained (Fig. 7); maximum potential magnitude range decreases to 3.8–7.4 assuming minimum $L_f/z_{max} = 1$ and maximum fault dip of 55°. A 3.9–8.0 Mw range is obtained assuming $L_f/z_{max} = 4$ and fault dip of 20° (Table1). The maximum magnitudes are predicted where the decollement depth (z_{max}) is deeper (Fig. 3): the front of the Apennines accretionary prism in the Po Plain (where the Emilia sequence took place in 2012 with Mw 6.1 and Mw 6 earthquakes); the Eastern Alps where the Mw 6.4 Friuli 1976 earthquake occurred. Magnitudes decrease moving toward the Adriatic Sea and the Ionian Sea (i.e., at the external thrust front). The southeast offshore Calabrian accretionary prism (notice that catalogs report only small earthquakes for this region) suffers from the absence of GPS data on the Ionian Sea used to interpolate the velocity field considered for magnitude calculation (great error due to unconstrained interpolation). This results in a very noisy map in those areas and where the larger magnitudes are predicted for thrust settings. Moderate seismicity ($4 < Mw < 5.5$) is recorded in the South Tyrrhenian Sea. The calculated maximum potential magnitude is consistent with the strongest thrust-fault earthquake known from historical catalogs (Mw 6.5 occurred in 1117 along the Southern Alps front; Guidoboni et al., 2005).

Maximum magnitudes in strike-slip areas are expected to vary between 5.6 and 7.6 (Fig. 8a). Considering a minimum fault dip angle of 45°, consistent with observations, the range decreases to 5.3–7.3 while it increases to 6.0–8.0 in case of faults dipping 85° and $L_f/z_{max} = 3$ (Table 1). A magnitude value of 6.7 is reported for the most energetic strike-slip earthquake in Italy (the 1627 Gargano earthquake Mw 6.6 ± 0.10; Rovida et al., 2021). Further, $M \geq 6$ has been experienced several times in southern Apennines and Sicily (Daunia 1361 Mw = 6.0; Gargano 1646 Mw = 6.7; Tavoliere delle Puglie 1731 Mw = 6.3; Melfi 1851 Mw = 6.5; Gondola 1893 Mw = 5.4; Patti gulf 1978 Mw = 6.1 - Rovida et al., 2021).

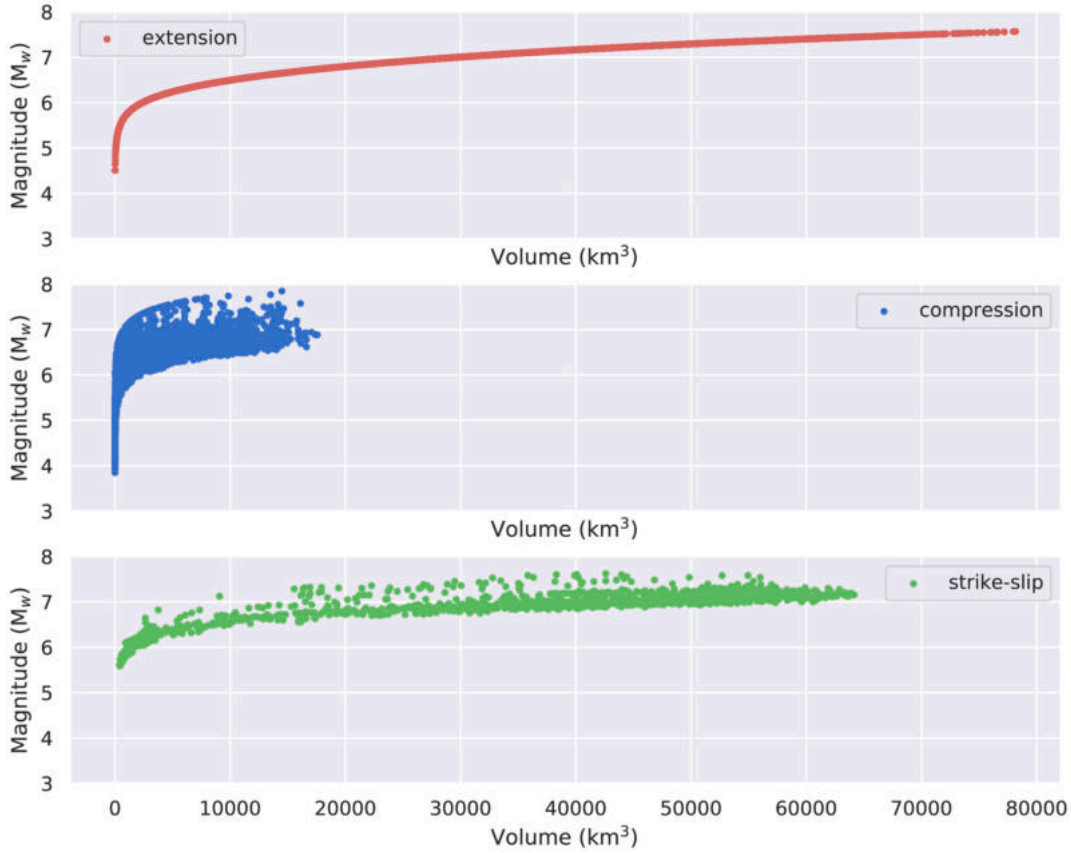

Fig. 6. Volume vs predicted magnitudes. The calculated magnitude at each node of the preferred model depends on the tectonic regime. In case of extensional tectonics, where the magnitude depends on the brittle volume and the gravitational potential, the graph is a curve (red curve). For compressional and strike-slip tectonics the same brittle volume can account for different values of maximum magnitudes depending on the strain rate, and the graphs occupy bands (blue for compression and green for strike-slip). (For interpretation of the references to colour in this figure legend, the reader is referred to the web version of this article.)

5. Discussions

The model presented here is based on the potential brittle volume concept and is time independent, i.e., magnitudes are calculated using physical parameters, regardless of the seismic catalogs. Our model provides a basis for seismic hazard assessment, alternative to those so far used as input required for the following techniques (e.g., PSHA, DSHA, NDSHA). The leading concept is that the brittle volume, during the interseismic period, is an accumulator of seismic energy, which is entirely dissipated at the coseismic stage. This energy is mainly elastic for thrusts and strike-slip faults, whereas it is gravitational for normal faults (Doglioni et al., 2015; Petricca et al., 2015, 2019, 2021). After calculating the volume potentially involved in faulting, it is possible to derive (by means of empirical relationships) the associated earthquake magnitudes (Bath and Duda, 1964; Petricca et al., 2015; Petricca et al., 2019).

Our results show that maximum possible magnitude increases with the assumed shape ratio factor (C) and with increasing fault dip angle in extensional and strike-slip settings, whereas it increases for decreasing fault dip angles in compressional settings (Table 1 and Table S3) as shown in Petricca et al. (2021). Predicted magnitudes vary in the range of ±0.77, ± 0.37 and ± 0.25 for normal, strike-slip and thrust fault earthquakes respectively. Magnitudes calculated at each node of our model grow exponentially with respect to brittle volume for normal faulting (red curve in Fig. 6). In the case of thrust and strike-slip faulting the magnitude calculated for a same brittle volume depends on the strain rate (i.e. the faster the deformation the larger the magnitude), and the exponential growth of the curves depicts bands instead of a simple curve (blue and green bands for compression and strike-slip respectively in Fig. 6); the wider the band the larger the range of variation in the strain rate and, consequently, the predicted magnitude. Lower values for the maximum possible magnitude are obtained in the thrust fault setting (Fig. 8a) since the decollement depth is on average shallower (≈1–17 km) than the BDT depth (≈4–23 km). Furthermore, the smaller magnitude observed in compressional areas are also due to lower strain rates than in extensional settings (Petricca et al., 2018). The predicted magnitudes are sensitive to the choice of initial parameters (fault dip [α] and geometry [L_f/z_{max}]) and to the tectonic regime. In fact, our map is intended as a fitting model with respect to a spectrum of variation of possible magnitude values. The total range of variation of predictions (Fig. 8a) is wider for normal faulting (up to 1.5 points for large magnitudes) than for strike-slip and thrust faulting (less than 0.8 points). The prediction of our preferred model (black line in Fig. 8a) is centered on the error band (green) related to strike-slip areas, whereas it is shifted to the lower part of the error band (red) for extensional areas, and to the upper part for compressional areas (blue band). Consequently, the maximum positive errors occur for normal faults (Fig. 8b) and the maximum negative errors for thrust faults (Fig. 8c).

Based on our best model, we perform a quantitative comparison among maximum magnitudes predicted by the present study with those 1) from seismic catalogs (CPTI15v3.0 - Rovida et al., 2021; CFTI5Med - Guidoboni et al., 2019), 2) from fault length-magnitude empirical relationships (Trippetta et al., 2019) and 3) from integrated studies (DISS 3.3.0 – DISS Working Group, 2021).

1) Model results are tested against the Italian seismicity with Mw ≥ 5.0 and depth ≤ 30 km collected in the CPTI15v3.0 (Rovida et al., 2021) covering the 1005–2019 time interval and the CFTI5Med (Guidoboni

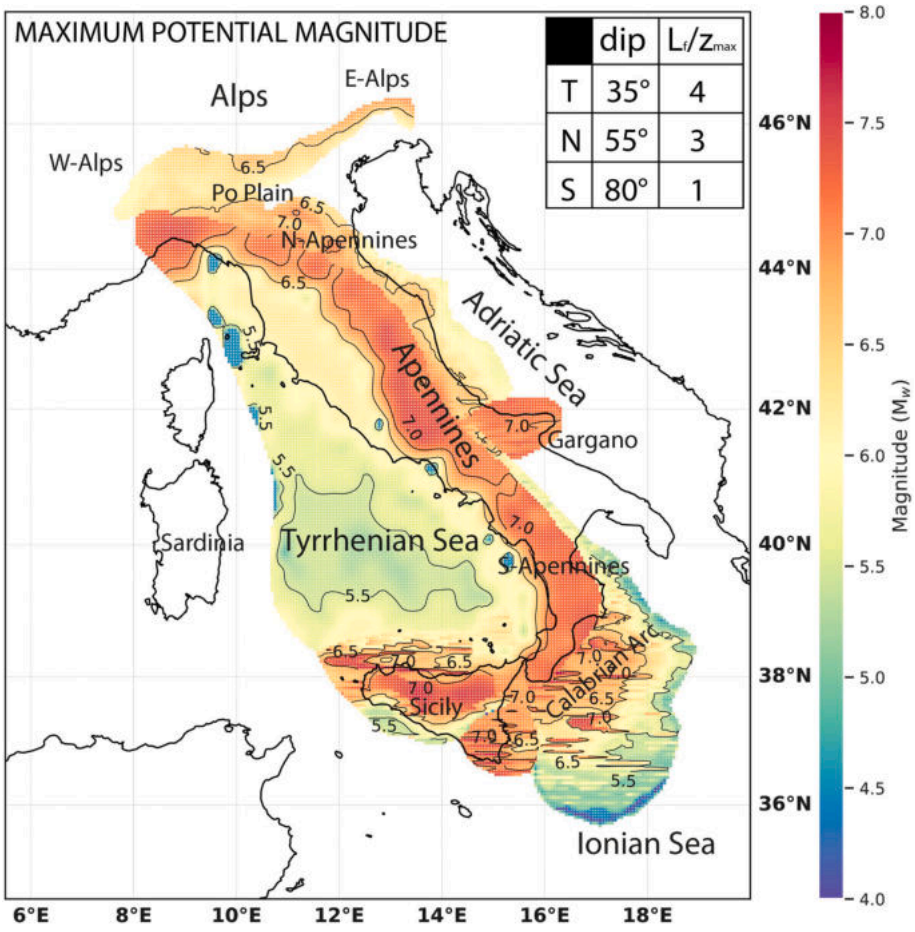

Fig. 7. Map of the maximum potential magnitude (M) predicted for the Italian territory due to normal, thrust and strike-slip faulting. M is calculated starting from the brittle volume and using the equation in Bath and Duda (1964) for thrust and strike-slip faults (governed by elastic energy) and the equation in Petricca et al. (2015) for normal faulting (governed by gravitational energy). Results assume the following fault dip α and $C = Lf/z_{max}$ (i.e. fault length - maximum faulting depth ratio): α =35° and C = 4 (thrust faults); α =55° and C = 3 (normal faults); α =80° and C = 1 (strike-slip faults).

et al., 2019) covering the 0–1997 time interval (Fig. 9a). The difference (**Δ**Mw) between magnitudes predicted by our model and observed magnitudes for the whole study domain are plotted in Fig. 9 against magnitude and year of occurrence of each event. The majority of historical/instrumental earthquakes are in agreement with predictions of our model (Fig. 9b-c). In some cases, the model, intended to predict maximum magnitude for a given location, overestimates magnitude of observed events. The model underestimates by 0.1–0.2 the magnitude of a few events along the Apennines chain and in the Tyrrhenian Sea, plus two events in Sicily. The magnitude of a thrust event occurred in 1117 (Veronese earthquake Mw 6.5 in Po Plain – Guidoboni et al., 2005) is underestimated by ≈0.28.

2) Trippetta et al. (2019), assuming that any fault can in principle be reactivated, compared the maximum magnitudes obtained by an extensive compilation of faults in Italy assessed by means of empirical relationships (Fault Length Earthquake Magnitude - FLEM) with magnitudes from national seismic catalogs. Their results show in most cases a good agreement between predicted and observed magnitudes, with differences that are in the ±1.0 range (in well-constrained areas) but almost always underestimating the observed value for Mw ≥6.5 (see their Fig. 13). By comparing magnitudes predicted by our study with FLEMs in Trippetta et al. (2019), it follows that magnitude estimates are larger for our model when Mw > 7.0, while larger FLEMs are given when Mw < 6.0. A good agreement between the two models is observed for 6.0 < Mw < 7.0, where the regression lines intercept the reference line (Fig. 10). The reason for underestimation of low magnitudes is that magnitudes obtained from fault lengths suffer the impossibility to resolve fault continuity and segmentation (i.e., the faults used for magnitude by Trippetta et al., 2019, could be segmented). In addition, the underestimation can be due to the lack of knowledge where detailed geologic studies (i.e. better estimates of fault dimensions) are not available.

3) Comparing our results with maximum magnitudes assigned to individual seismogenic sources (ISSs) of the DISS (DISS Working Group, 2021 – Table S4) the following strengths and weaknesses of our method emerge (Fig. 11a-b). Pros: i) as conservative as they were intended to be, our predicted magnitudes are larger than those of earthquakes that occurred both in historical and instrumental epochs. This is especially true for normal and strike-slip earthquakes whose magnitude mainly depends on the BDT depth, well-defined for the Italian territory; ii) the overestimation with respect of magnitudes defined for historic and instrumental events decreases moving from high (max overestimation ≈ +1.5) to low (max overestimation ≈ +0.5) magnitude earthquakes (see colored lines in Fig. 11a-b). In few cases, the magnitudes reported in the DISS ISSs are larger than those predicted by our model. However, these earthquakes are associated with sources that produced their last earthquake before the XIX century. Overall, our model overestimates magnitudes and, consequently, should account also for uncharacteristic earthquakes (e.g. Geller et al., 2015 and references therein); iii) in Italy larger magnitudes are predicted for normal, intermediate for strike-slip and lower for thrust faults earthquakes, fitting DISS predictions. Cons: an underestimation of large magnitudes (M > 6.0) emerges for thrust fault earthquakes. Worth of notice is that thrust earthquakes larger than 6.5 are still not recorded instrumentally, so far. It cannot be excluded that such inconsistency may result from the overestimation of magnitudes in historic catalogs based on macroseismic estimation. Our underestimation could also be related to large error (– a few km) in the definition of the maximum thrust decollement depth (see

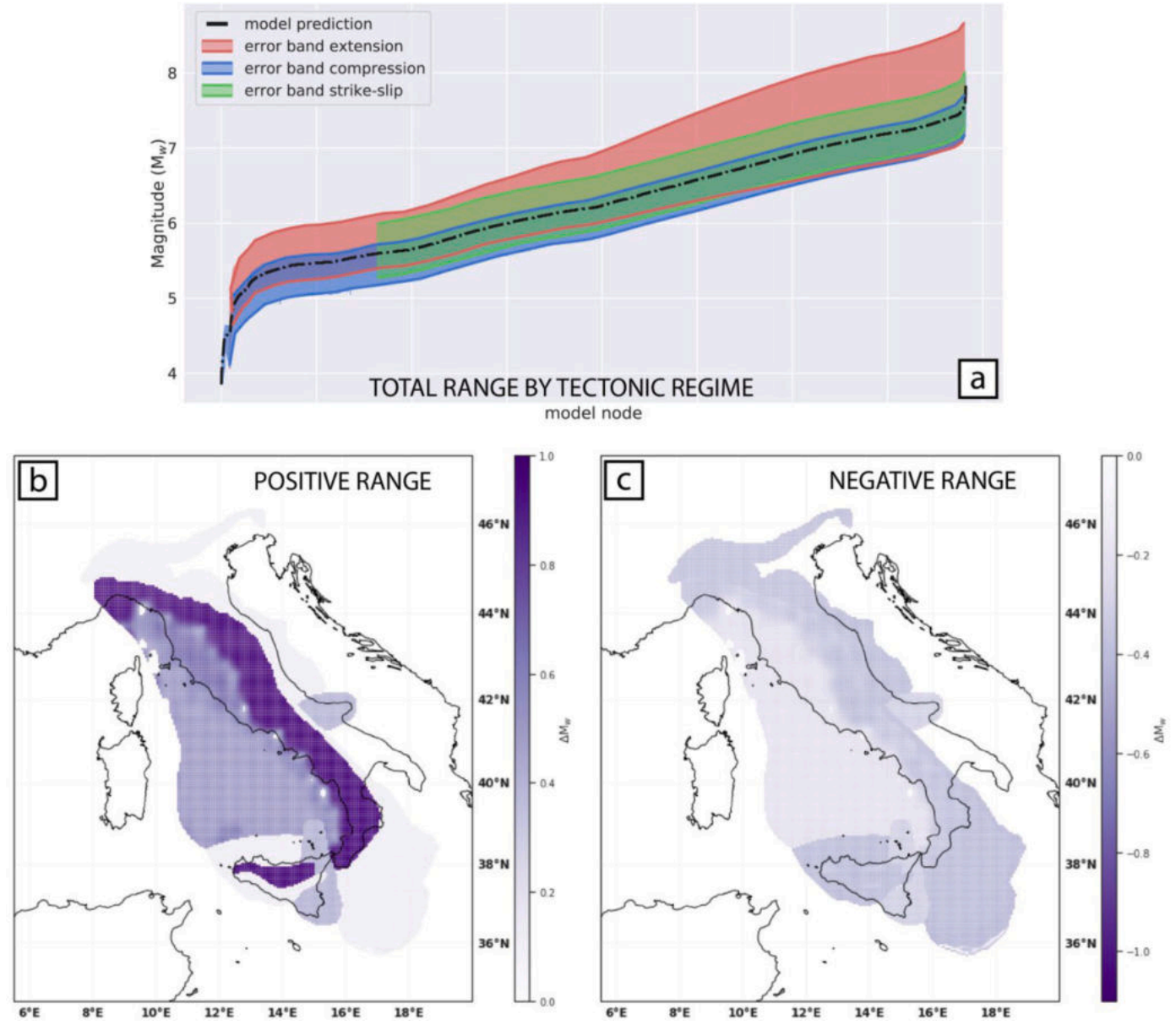

Fig. 8. **a)** Range of variation of predicted magnitudes (red band = normal; blue band = thrust; green band = strike-slip) for different initial parameters varied from - MINIMUM: α =55° and C = 1 (thrust faults); α =20° and C = 1 (normal faults); α =45° and C = 1 (strike-slip faults); – MAXIMUM: α =20° and C = 4 (thrust faults); α =85° and C = 3 (normal faults); α =85° and C = 3 (strike-slip faults). **b)** and **c)** show the positive and negative range of variation in predicted magnitudes when varying the initial parameters. (For interpretation of the references to colour in this figure legend, the reader is referred to the web version of this article.)

Petricca et al., 2019). Notice that each individual seismogenic source (ISS) of the DISS is associated with a composite seismogenic source (CSS) that may include one or more individual sources characterized by homogeneous parametrization (see Basili et al., 2008 for details). In the last release of the DISS (v3.3.0) a new magnitude for CSSs is calculated based on scaling relation from Leonard (2014), a step in the direction of an increase in the maximum magnitude values. In Fig. 11c and d, we provide another comparison between magnitudes predicted by our preferred model and the magnitude assigned to composite seismogenic sources (CSS), highlighting how the differences between the two models are in the range of ±0.5.

The Italian Seismic Hazard Model MPS19 (Meletti et al., 2021; Visini et al., 2021) estimates the maximum magnitude for 18 tectonically homogeneous macro-areas by selecting the maximum value reported in the CPTI15 catalog (Rovida et al., 2021) and the value reported in the ISS of the DISS database (DISS Working Group, 2021), assigning to each area the largest value between the two magnitudes. This raises the point of what level of hazard must be considered, that is a questionable and subjective decision especially in PSHA, since improper selection of parameters may lead to either unsafe or overly conservative designs. As it emerges from this discussion, the maximum magnitude is a prime parameter that, in our opinion, should be as conservative as possible as our method has demonstrated to be. Our model tendency to overestimation of magnitudes may occur because of involved brittle volumes smaller than expected. This may be due to faults detached at levels shallower than the brittle ductile transition, or to fault aseismic behavior. Further, the calculation for extensional tectonic regimes depends on the radiation coefficient that we kept equal to 1.0 but could be much smaller (down to 0.03; Choy and Boatwright, 1995), thus reducing the magnitude value by ≈1. However, strong or major earthquakes should not be excluded as in case they could have longer recurrence time (not recorded yet).

In seismic areas earthquakes recurrence depends on the velocity at

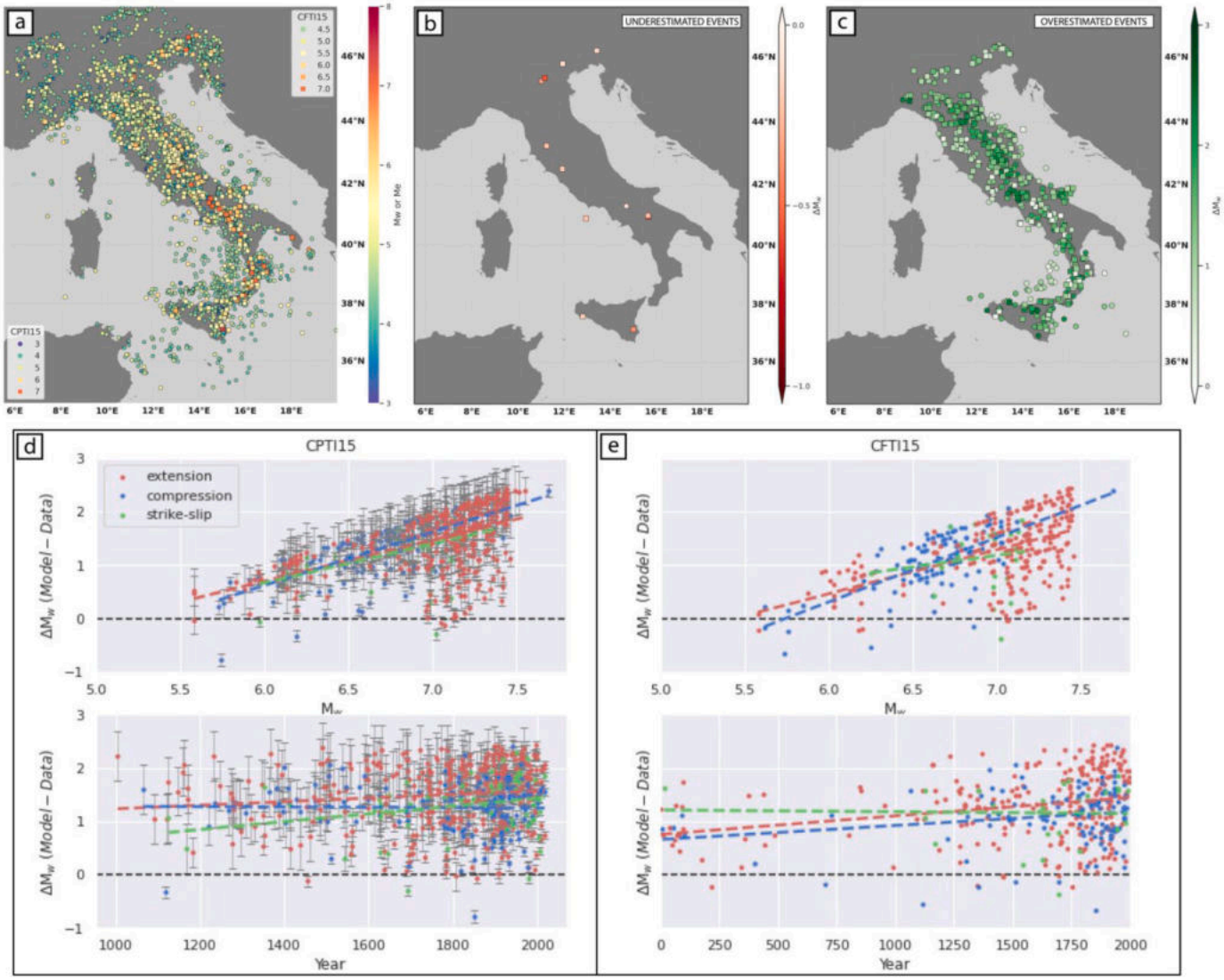

Fig. 9. a) Italian seismicity in the 0–2019 019 time-window with Mw ≥3.5 and depth ≤ 30 km (from CPTI15v3.0; Rovida et al., 2021 [circles] and CFTI15Med; Guidoboni et al., 2019 [squares]) used to test model results. For the whole study domain, the difference (ΔMw) between predicted magnitudes and observed magnitudes are plotted vs magnitude and year of occurrence of each event (graphs in the lower part) for **d)** CPTI15 and **e)** CFTI catalogs. The model overestimates low magnitudes more in case of extensional events (red circles) with respect to thrust events (blue circles). Notice that model predictions do not correlate with the year of occurrence following the significant increase of observations. Gray bars indicate the error associated with observed magnitude estimation available in CPT115v3.0 but not in the CFTI5Med. **b)** and **c)** deltas of predicted magnitudes minus observed magnitudes for the whole study domain show regions where our model underestimates (red points) or correctly predicts (green points) the observed magnitudes. Few events align along the Apennine and in the Tyrrhenian Sea plus two events in Sicily underestimating in the order of 0.1–0.2. One thrust event that occurred in 1117 (Veronese earthquake Mw 6.5 in Po Plain) is underestimated by ≈0.28 point of magnitude. (For interpretation of the references to colour in this figure legend, the reader is referred to the web version of this article.)

which deformation, currently, takes place. Low magnitude earthquakes occur at all observed strain rates, while larger magnitudes occur at low strain rates only. In fact, Riguzzi et al. (2012) observed for Italy that past earthquakes with magnitudes >5.0 occurred where geodetic strain rate (SR) is <20 nanostrain/yr, while M is limited to 5.0 where SR > 20 nanostrain/yr. Further, SR =40 nanostrain/yr is, for Italy, the bound value separating areas characterized by significant seismic activity from those affected by background seismicity (Riguzzi et al., 2012). However, small strain rates imply that the recurrence interval of large events would be very large.

According to Riguzzi et al. (2012) future earthquakes are more likely to occur sooner in regions with low SR (i.e., regions having the same tectonic regime and geodetic velocity, but relatively lower strain; gray areas in Fig. 12), having longer recurrence time for contractional settings (Riguzzi et al., 2012). High strain rates (>20 nanostrain/yr) lead to lower probability to generate strong earthquakes soon and are observed in regions struck by important seismic sequences in the last century (i.e., Friuli 1976 in the Eastern Alps; Emilia 2012 in the Po Plain; Fucino 1915, Irpinia 1980, Colfiorito 1997, L'aquila 2009 and central Italy in 2016 along the Apennine extensional belt, 1905–1908 in Calabria and Sicily; see Fig. 1 and red areas in Fig. 12). This information can be integrated with our M_{max} predictions. In terms of hazard, we expect large earthquakes to occur in low strain rate areas only if there is a potential of Mw > 5 in our map. Large magnitudes are expected due to low strain rate in the compressional part of northern Italy ($5 < M_w < 6.5$). Earthquakes of magnitude 5 < Mw < 6.5–7.0 are expected in central Calabria (extension) and Ionian off-shore (compression) where the higher strain is recorded in the accretionary prism of the Calabria subduction. Magnitudes between 5.8 and 6.0 are likely to occur in contractional regions in the Adriatic Sea. Notice that slow strain rates are associated with shallower depth of the decollement layer for thrusts (Petricca et al., 2018), hence limiting the maximum value for earthquake magnitudes.

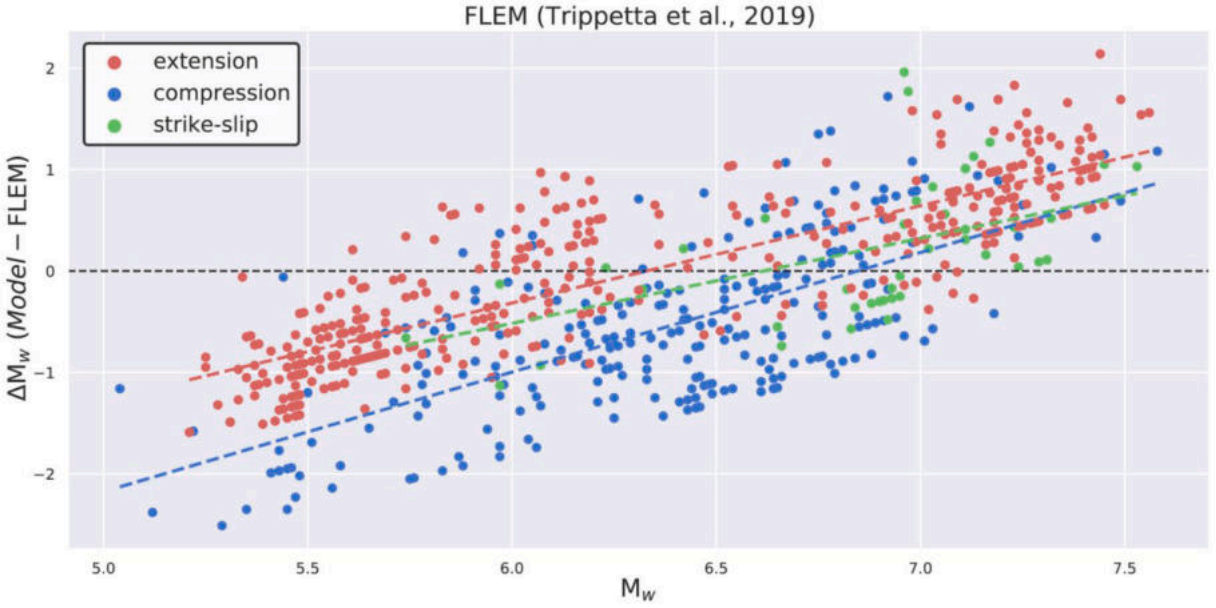

Fig. 10. Comparison between magnitudes obtained from fault length - magnitude scaling relationships (FLEM - Fault Length Earthquake Magnitude) by Trippetta et al. (2019) compilation and magnitudes obtained at the same location from our calculations presented in Fig. 7. Regression lines are represented with dotted traces colored according to the faulting regime.

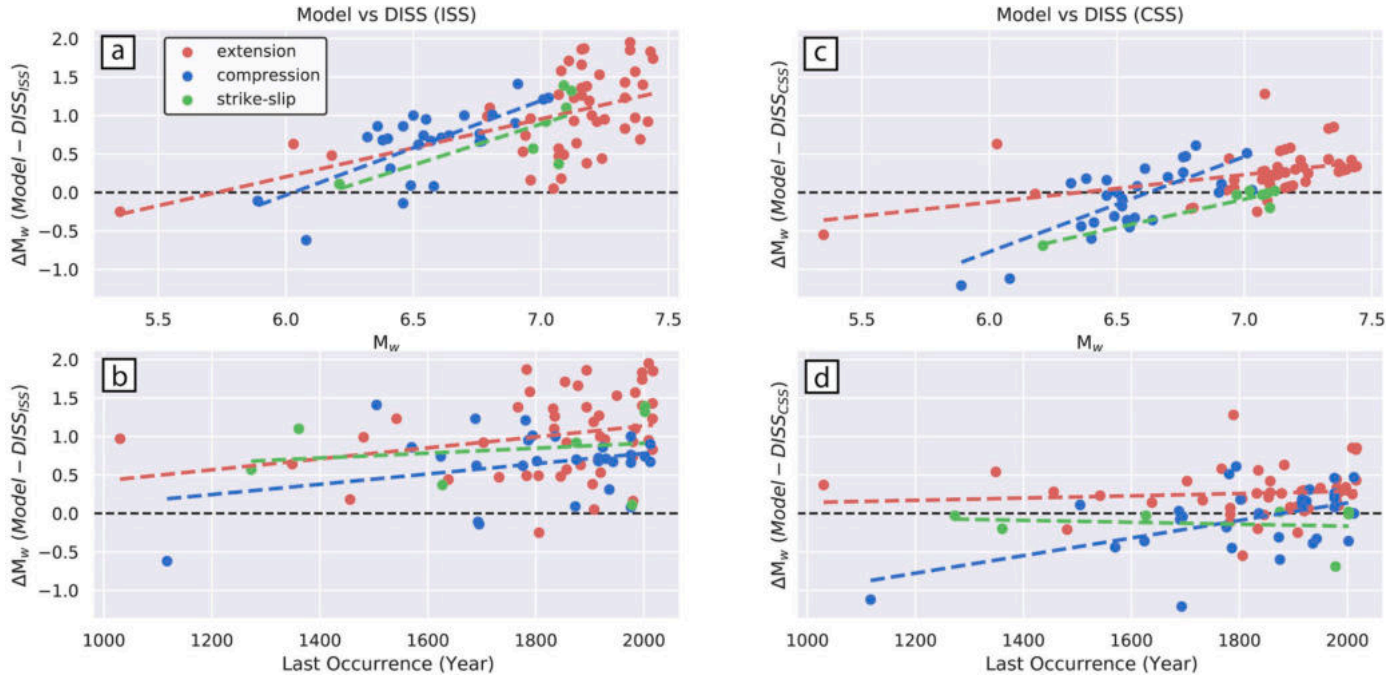

Fig. 11. a) Comparison between magnitudes obtained from DISS compilation considering Individual seismogenic sources (DISS Working Group, 2021) and magnitudes obtained at the same location from our calculations presented in Fig. 7. Regression lines are represented with dotted traces colored according to the faulting regime. **b)** Differences between our model and the DISS model are plotted versus the year of last occurrence of the earthquake triggered by the considered seismogenic source. **c)** and **d)** Same comparison between our results and magnitudes obtained from DISS compilation, in this case considering the Composite Seismogenic Sources.

Further, a thin crust prevents the occurrence of crustal earthquakes with $M_w > 5$ in the extensional setting of the Tyrrhenian Sea.

It should finally be noted that there are few regions along the central-northern Apennines extensional chain where Mw7 are predicted by our model, and that have not yet experienced strong earthquakes in the recent period (compare gray areas in Fig. 12 with the same points in Fig. 7). These areas are located north of the 1997, 2009 and 2016 seismic sequences of Central Italy (events 8, 9, 11 and 12 in Fig. 1). Notice that the definition of the strain rate strictly depends on the GPS network density, accuracy, time-span and it is not homogeneous within the territory. This makes our indication just preliminary with no intentions to provide a time for the occurrence of the next earthquake.

6. Conclusions

A theoretical model aimed at providing values for the maximum

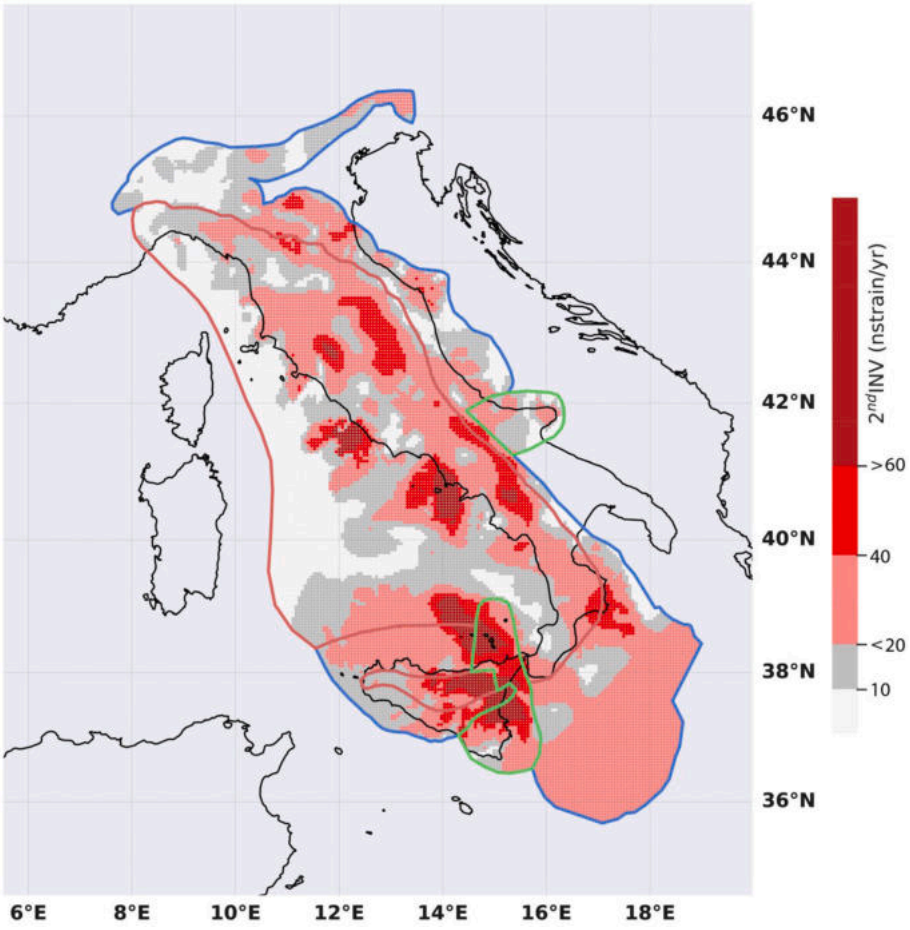

Fig. 12. 2nd invariant of the strain rate from GPS data (Devoti et al., 2017). Low magnitude earthquakes are expected to occur at all strain rates, while large magnitudes occur in areas with relative lower strain rate, particularly where there are strain rate gradients (Riguzzi et al., 2012). Red, green and blue solid lines delimit areas of extensional, strike-slip and thrust tectonics respectively. (For interpretation of the references to colour in this figure legend, the reader is referred to the web version of this article.)

possible magnitude is proposed and applied to the Italian area. The maximum possible magnitude is calculated on available brittle volumes obtained considering active thrusts decollement depths (in compressional areas) or brittle-ductile transition depths (in extensional and strike-slip areas). Maximum magnitudes depend on elastic energy and therefore on strain rates for thrusts and strike-slip faults, and on gravitational energy for normal faults. The magnitudes are proportional to the ratio between fault lengths and the maximum depth of faulting. The Maximum magnitudes are calculated utilizing empirical relationships and presented in a single map. The largest predicted values are 7.3 $\pm$ 0.25 for thrust faulting, 7.6 $\pm$ 0.77 for normal faulting and 7.6 $\pm$ 0.37 for strike-slip faulting. These values are higher with respect to the largest magnitude of thrust (Mw 6.5–6.7), normal (7.3) and strike-slip (Mw 6.7) related earthquakes recorded in Italy. This could be interpreted as related to two possibilities, i.e., 1) an overestimation of the computed volume due, for example, to decollement layers shallower than the BDT, or 2) a longer recurrence time of strong and major earthquakes that have not yet occurred in the Italian historical record. The occurrence of earthquakes with a given magnitude may be related to current strain rates. The combination of our map of maximum possible magnitude with the map of current strain rates by Devoti et al. (2017) shows that a large part of the Italian territory is prone to earthquakes with M $>$ 5 in the near future.

Credit statement

Patrizio Petricca: Conceptualization, Methodology, Software, Data curation, Writing- Original draft preparation, Visualization, Formal analysis, Supervision. Eugenio Carminati: Conceptualization, Writing-Reviewing and Editing. Carlo Doglioni: Conceptualization, Writing-Reviewing and Editing.

Declaration of Competing Interest

We wish to confirm that there are no known conflicts of interest associated with this publication.

Acknowledgments

Fig. 1 was produced using the GMT software (http://gmt.soest.hawaii.edu/); the remaining figures using Matplotlib. Tables with data used to produce the maps, plots and results are uploaded as Supporting Information. Federica Riguzzi is warmly thanked for providing GPS data. Comments from the editor Ling Chen, Mircea Radulian and two anonymous reviewers greatly improved this paper. Thanks to Davide Zaccagnino for fruitful comments that improved the manuscript. Funding by Progetti di Ateneo Sapienza (2019 and 2021 for EC and 2018 for CD) is acknowledged.

Appendix A. Supplementary data

Supplementary data to this article can be found online at https://doi.org/10.1016/j.tecto.2022.229405.

References

Aki, K., 1984. Asperities, barriers, characteristic earthquakes and strong motion prediction. J. Geophys. Res. Solid Earth 89 (B7), 5867–5872. https://doi.org/10.1029/JB089iB07p05867.

Aki, K., Richards, P., 1980. Quantitative Seismology. W.H. Freeman, New York.

Amato, A., Azzara, R., Chiarabba, C., Cimini, G.B., Cocco, M., Di Bona, M., et al., 1998. The 1997 Umbria-Marche, Italy, earthquake sequence: a first look at the main shocks and aftershocks. Geophys. Res. Lett. 25 (15), 2861–2864. https://doi.org/10.1029/98GL51842.

Anderson, E.M., 1951. The Dynamics of Faulting. Oliver & Boyd, Edinburgh.

Argnani, A., Frugoni, F., Cosi, R., Ligi, M., Favali, P., 2001. Tectonics and Seismicity of the Apulian Ridge South of Salento Peninsula (Southern Italy).

Atkinson, G.M., 2004. An overview of developments in seismic hazard analysis. In: In the 13th World Conference on Earthquake Engineering, pp. 1–6.

Basili, R., Valensise, G., Vannoli, P., Burrato, P., Fracassi, U., Mariano, S., et al., 2008. The Database of Individual Seismogenic sources (DISS), version 3: summarizing 20 years of research on Italy's earthquake geology. Tectonophysics 453 (1–4), 20–43. https://doi.org/10.1016/j.tecto.2007.04.014.

Basili, R., Kastelic, V., Demircioglu, M.B., Garcia, Moreno D., Nemser, E.S., Petricca, P., Sboras, S.P., Besana-Ostman, G.M., Cabral, J., Camelbeeck, T., Caputo, R., Danciu, L., Domac, H., Fonseca, J., García-Mayordomo, J., Giardini, D., Glavatovic, B., Gulen, L., Ince, Y., Pavlides, S., Sesetyan, K., Tarabusi, G., Tiberti, M. M., Utkucu, M., Valensise, G., Vanneste, K., Vilanova, S., Wössner, J.. The European Database of Seismogenic Faults (EDSF) compiled in the framework of the Project SHARE. *http://diss.rm.ingv.it/share-edsf/*.

Bath, M., Duda, S.J., 1964. Earthquake volume, fault plane area, seismic energy, strain, deformation and related quantities. Ann. Geophys. 17, 353–368.

Bignami, C., Valerio, E., Carminati, E., Doglioni, C., Petricca, P., Tizzani, P., Lanari, R., 2020. Are normal fault earthquakes due to elastic rebound or gravitational collapse? Ann. Geophys. 63 (2), SE213. https://doi.org/10.4401/ag-8455.

Byerlee, J., 1978. Friction of rocks. Pure Appl. Geophys. 116 (4–5), 615–626.

Caputo, M., 1976. The area of the fault, the dislocation, the stress drop and the seismic moment of the Friuli earthquake of May 6th, 1976. Ann. Geophys. 29 (3), 171–177.

Carafa, M.M., Barba, S., 2011. Determining rheology from deformation data: the case of Central Italy. Tectonics 30 (2). https://doi.org/10.1029/2010TC002680.

Carminati, E., Doglioni, C., 2012. Alps Vs. Apennines: the paradigm of a tectonically asymmetric Earth. Earth-Sci. Rev. 112, 67–96. https://doi.org/10.1016/j.earscirev.2012.02.004.

Carminati, E., Doglioni, C., Barba, S., 2004. Reverse migration of seismicity on thrusts and normal faults. Earth-Sci. Rev. 65, 195–222. https://doi.org/10.1016/S0012-8252(03)00083-7.

Carminati, E., Bignami, C., Doglioni, C., Smeraglia, L., 2020. Lithological control on multiple surface ruptures during the 2016-2017 Amatrice-Norcia seismic sequence. J. Geodyn. 134, 101676 https://doi.org/10.1016/j.jog.2019.101676.

Cassano, E., Anelli, L., Fichera, R., Cappelli, V., 1986. Pianura Padana, interpretazione integrata di dati geofisici e geologici. AGIP, San Donato Milanese, p. 27.

Casula, G., Cherchi, A., Montadert, L., Murru, M., Sarria, E., 2001. The Cenozoic graben system of Sardinia (Italy): geodynamic evolution from new seismic and field data. Mar. Pet. Geol. 18 (7), 863–888. https://doi.org/10.1016/S0264-8172(01)00023-X.

Chiarabba, C., Amato, A., Anselmi, M., Baccheschi, P., Bianchi, I., Cattaneo, M., et al., 2009. The 2009 L'Aquila (Central Italy) MW 6.3 earthquake: Main shock and aftershocks. Geophys. Res. Lett. 36 (18) https://doi.org/10.1029/2009GL039627.

Chiaraluce, L., Di Stefano, R., Tinti, E., Scognamiglio, L., Michele, M., Casarotti, E., et al., 2017. The 2016 Central Italy seismic sequence: a first look at the mainshocks, aftershocks, and source models. Seismol. Res. Lett. 88 (3), 757–771. https://doi.org/10.1785/0220160221.

Choy, G.L., Boatwright, J.L., 1995. Global patterns of radiated seismic energy and apparent stress. J. Geophys. Res. 100 (B9), 18205–18228. https://doi.org/10.1029/95JB01969.

Della Vedova, B., Bellani, S., Pellis, G., Squarci, P., 2001. Deep temperatures and surface heat flow distribution. In: Anatomy of an Orogen: The Apennines and Adjacent Mediterranean Basins. Springer, Dordrecht, pp. 65–76.

Devoti, R., D'Agostino, N., Serpelloni, E., Pietrantonio, G., Riguzzi, F., Avallone, A., et al., 2017. A combined velocity field of the Mediterranean region. Ann. Geophys. 60 (2), 0215. https://doi.org/10.4401/ag-7059.

DISS Working Group, 2021. Database of Individual Seismogenic Sources (DISS), Version 3.3.0: A compilation of potential sources for earthquakes larger than M 5.5 in Italy and surrounding areas. https://doi.org/10.13127/diss3.3.0.

Doglioni, C., Carminati, E., 2008. Structural styles and Dolomites field trip. Mem. Descr. Carta Geol. It. 82, 1–299.

Doglioni, C., Barba, S., Carminati, E., Riguzzi, F., 2011. Role of the brittle-ductile transition on fault activation. Phys. Earth Planet. Inter. 184, 160–171.

Doglioni, C., Carminati, E., Petricca, P., Riguzzi, F., 2015. Normal fault earthquakes or graviquakes. Sci. Rep. 5, 12110. https://doi.org/10.1038/srep12110.

Dziewonski, A.M., Anderson, D.L., 1981. Preliminary reference Earth model. Phys. Earth Planet. Inter. 25 (4), 297–356.

Farolfi, G., Del Ventisette, C., 2017. Strain rates in the Alpine Mediterranean region: Insights from advanced techniques of data processing. GPS Solutions 21 (3), 1027–1036. https://doi.org/10.1007/s10291-016-0588-z.

Fracassi, U., Valensise, G., 2007. Unveiling the sources of the catastrophic 1456 multiple earthquake: Hints to an unexplored tectonic mechanism in southern Italy. Bull. Seismol. Soc. Am. 97 (3), 725–748. https://doi.org/10.1785/0120050250.

Galli, P., Naso, G., 2008. The "taranta" effect of the 1743 earthquake in Salento (Apulia, Southern Italy). Boll. Geofis. Teor. Appl. 49 (2), 177–204.

Geller, R.J., Mulargia, F., Stark, P.B., 2015. Why we need a new paradigm of earthquake occurrence. Subduction dynamics: From mantle flow to mega disasters. Geophys. Monogr. 211, 183–191.

Govoni, A., Marchetti, A., De Gori, P., Di Bona, M., Lucente, F.P., Improta, L., et al., 2014. The 2012 Emilia seismic sequence (Northern Italy): Imaging the thrust fault system by accurate aftershock location. Tectonophysics 622, 44–55. https://doi.org/10.1016/j.tecto.2014.02.013.

Guidoboni, E., Comastri, A., Boschi, E., 2005. The "exceptional" earthquake of 3 January 1117 in the Verona area (northern Italy): a critical time review and detection of two lost earthquakes (lower Germany and Tuscany). J. Geophys. Res. 110, B12309. https://doi.org/10.1029/2005JB003683.

Guidoboni, E., Ferrari, G., Tarabusi, G., Sgattoni, G., Comastri, A., Mariotti, D., Ciuccarelli, C., Bianchi, M.G., Valensise, G., 2019. CFTI5Med, the new release of the catalogue of strong earthquakes in Italy and in the Mediterranean area. Sci. Data 6 (80). https://doi.org/10.1038/s41597-019-0091-9.

Hyndman, R.D., Yamano, M., Oleskevich, D.A., 1997. The seismogenic zone of subduction thrust faults. Island Arc 6 (3), 244–260. https://doi.org/10.1111/j.1440-1738.1997.tb00175.x.

Jimenez, M.J., Giardini, D., Grünthal, G., SESAME Working Group, 2001. Unified seismic hazard modelling throughout the Mediterranean region. Boll. Geofis. Teor. Appl. 42 (1–2), 3–18.

Kammerer, A.M., Ake, J.P., 2012. Practical Implementation Guidelines for SSHAC Level 3 and 4 Hazard Studies, Office of Nuclear Regulatory Research. U.S. Nuclear Regulatory Commission, NUREG-2117, Rev. 1.

Leonard, M., 2010. Earthquake fault scaling: Self-consistent relating of rupture length, width, average displacement, and moment release. Bull. Seismol. Soc. Am. 100 (5A), 1971–1988. https://doi.org/10.1785/0120090189.

Leonard, M., 2014. Self-Consistent Earthquake Fault-Scaling Relations: Update and Extension to Stable Continental Strike-Slip Faults. Bull. Seismol. Soc. Am. https://doi.org/10.1785/0120140087.

Mai, P.M., Beroza, G.C., 2000. Source scaling properties from finite-fault-rupture models. Bull. Seismol. Soc. Am. 90 (3), 604–615. https://doi.org/10.1785/0119990126.

Malinverno, A., Ryan, W.B.F., 1986. Extension in the Tyrrhenian Sea and shortening in the Apennines as a result of arc migration driven by sinking of the lithosphere. Tectonics 5, 227–245. https://doi.org/10.1029/TC005i002p00227.

Mele, G., Di Luzio, E., Di Salvo, C., 2013. Mapping Moho depth variations in Central Italy from PsMoho-P delay times: evidence of an E-W transition in the Adriatic Moho at 42° N latitude. Geochem. Geophys. Geosyst. 14 (10), 3929–3938. https://doi.org/10.1002/ggge.20235.

Meletti, C., Marzocchi, W., D'Amico, V., Lanzano, G., Luzi, L., Martinelli, F., et al., 2021. The new Italian seismic hazard model (MPS19). Ann. Geophys. https://doi.org/10.4401/ag-8579.

Merlini, S., Doglioni, C., Fantoni, R., Ponton, M., 2002. Analisi strutturale lungo un profilo geologico tra la linea Fella-Sava e l'avampaese adriatico (Friuli Venezia Giulia-Italia). Mem. Soc. Geol. It. 57, 293–300.

Mohammed, T., Atkinson, G.M., Assatourians, K., 2014. Uncertainty in recurrence rates of large magnitude events due to short historic catalogs. J. Seismol. 18 (3), 565–573. https://doi.org/10.1007/s10950-014-9428-1.

Nappi, R., Gaudiosi, G., Alessio, G., De Lucia, M., Porfido, S., 2017. The environmental effects of the 1743 Salento earthquake (Apulia, southern Italy): a contribution to seismic hazard assessment of the Salento Peninsula. Nat. Hazards 86 (2), 295–324. https://doi.org/10.1007/s11069-016-2548-x.

Ohnaka, M., 1976. A physical basis for earthquakes based on the elastic rebound model. Bull. Seismol. Soc. Am. 66 (2), 433–451.

Panza, G.F., Bela, J., 2020. NDSHA: a new paradigm for reliable seismic hazard assessment. Eng. Geol. 275, 105403.

Petersen, M.D., Moschetti, M.P., Powers, P.M., Mueller, C.S., Haller, K.M., Frankel, A.D., et al., 2015. The 2014 United States national seismic hazard model. Earthquake Spectra 31 (1_suppl), S1–S30. https://doi.org/10.1193/120814EQS210M.

Petricca, P., Carafa, M.M., Barba, S., Carminati, E., 2013. Local, regional, and plate scale sources for the stress field in the Adriatic and Periadriatic region. Mar. Pet. Geol. 42, 160–181. https://doi.org/10.1016/j.marpetgeo.2012.08.005.

Petricca, P., Barba, S., Carminati, E., Doglioni, C., Riguzzi, F., 2015. Graviquakes in Italy. Tectonophysics 656, 202–214. https://doi.org/10.1016/j.tecto.2015.07.001.

Petricca, P., Carminati, E., Doglioni, C., Riguzzi, F., 2018. Brittle-ductile transition depth versus convergence rate in shallow crustal thrust faults: considerations on seismogenic volume and impact on seismicity. Phys. Earth Planet. Inter. 284, 72–81. https://doi.org/10.1016/j.pepi.2018.09.002.

Petricca, P., Carminati, E., Doglioni, C., 2019. The Decollement depth of active thrust faults in Italy: implications on potential earthquake magnitude. Tectonics 38 (11), 3990–4009. https://doi.org/10.1029/2019TC005641.

Petricca, P., Bignami, C., Doglioni, C., 2021. The epicentral fingerprint of earthquakes marks the coseismically activated crustal volume. Earth Sci. Rev. 218, 103667 https://doi.org/10.1016/j.earscirev.2021.103667.

Pezzo, G., et al., 2020. Active fold-thrust belt to foreland transition in Northern Adria, Italy, tracked by seismic reflection profiles and GPS offshore data. Tectonics 39 (11) e2020TC006425.

Pondrelli, S., Salimbeni, S., Ekström, G., Morelli, A., Gasperini, P., Vannucci, G., 2006. The Italian CMT dataset from 1977 to the present. Phys. Earth Planet. Inter. 159 (3–4), 286–303. https://doi.org/10.1016/j.pepi.2006.07.008.

Reid, H.F., 1910. The California earthquake of April 18, 1906, Report of the State Investigation Commission, Vol. 2. Carnegie Institution of Washington.

Riguzzi, F., Crespi, M., Devoti, R., Doglioni, C., Pietrantonio, G., Pisani, A.R., 2012. Geodetic strain rate and earthquake size: New clues for seismic hazard studies. Phys. Earth Planet. Inter. 206-207, 67–75.

Rovida, A., Locati, M., Camassi, R., Lolli, B., Gasperini, P., Antonucci, A., 2021. Catalogo Parametrico dei Terremoti Italiani (CPTI15), versione 3.0. In: Istituto Nazionale di Geofisica e Vulcanologia (INGV). https://doi.org/10.13127/CPTI/CPTI15.3.

Schirripa Spagnolo, G., Mercuri, M., Billi, A., Carminati, E., Galli, P., 2021. The segmented Campo Felice normal faults: seismic potential appraisal by application of empirical relationships between rupture length and earthquake magnitude in the central Apennines, Italy. Tectonics 40 (7). https://doi.org/10.1029/2020TC006465 e2020TC006465.

Scholz, C.H., 2019. The mechanics of earthquakes and faulting. Cambridge University Press 1–493.
Schönborn, G., 1999. Balancing cross sections with kinematic constraints: the Dolomites (northern Italy). Tectonics 18 (3), 527–545.
Schwartz, D.P., 2018. Past and future fault rupture lengths in seismic source characterization-the long and short of it. Bull. Seismol. Soc. Am. 108 (5A), 2493–2520. https://doi.org/10.1785/0120160110.
Schwartz, D.P., Coppersmith, K.J., 1984. Fault behavior and characteristic earthquakes - examples from the Wasatch and San Andreas fault zones. J. Geophys. Res. 89, 5681–5698. https://doi.org/10.1029/JB089iB07p05681.
Scrocca, D., 2006. Thrust front segmentation induced by differential slab retreat in the Apennines (Italy). Terra Nova, 2006 18 (2), 154–161.
Stirling, M., McVerry, G., Gerstenberger, M., Litchfield, N., Van Dissen, R., Berryman, K., et al., 2012. National seismic hazard model for New Zealand: 2010 update. Bull. Seismol. Soc. Am. 102 (4), 1514–1542. https://doi.org/10.1785/0120110170.
Thingbaijam, K.K.S., Martin Mai, P., Goda, K., 2017. New empirical earthquake source-scaling laws. Bull. Seismol. Soc. Am. 107 (5), 2225–2246. https://doi.org/10.1785/0120170017.
Trippetta, F., Petricca, P., Billi, A., Collettini, C., Cuffaro, M., Lombardi, et al., 2019. From mapped faults to fault-length earthquake magnitude (FLEM): a test on Italy with methodological implications. Solid Earth 10 (5), 1555–1579. https://doi.org/10.5194/se-10-1555-2019.
Valensise, G., Pantosti, D., Basili, R., 2004. Seismology and tectonic setting of the 2002 Molise, Italy, earthquake. Earthquake Spectra 20 (1_suppl), 23–37. https://doi.org/10.1193/1.1756136.
Visini, F., Pace, B., Meletti, C., Marzocchi, W., Akinci, A., Azzaro, R., et al., 2021. Earthquake Rupture forecasts for the MPS19 Seismic Hazard Model of Italy. Ann. Geophys. 64 (2) https://doi.org/10.4401/ag-8608. SE220-SE220.
Wells, D.L., Coppersmith, K.J., 1994. New empirical relationships among magnitude, rupture length, rupture width, rupture area, and surface displacement. Bull. Seismol. Soc. Am. 84 (4), 974–1002.
Woessner, J., Laurentiu, D., Giardini, D., Crowley, H., Cotton, F., Grünthal, G., et al., 2015. The 2013 European seismic hazard model: key components and results. Bull. Earthq. Eng. 13 (12), 3553–3596. https://doi.org/10.1007/s10518-015-9795-1.
Wyss, M., 2015. Testing the basic assumption for probabilistic seismic-hazard assessment: 11 failures. Seismol. Res. Lett. 86 (5), 1405–1411. https://doi.org/10.1785/0220150014.